Available online at www.sciencedirect.com

ScienceDirect

journal homepage: www.elsevier.com/locate/jasi

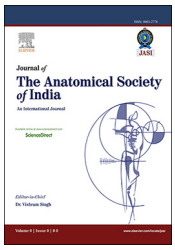

Vector analysis of porosity evidences bone loss at the epiphysis in the BTX rat model of disuse osteoporosis

D. Chappard *, *H. Libouban*

GEROM Groupe Etudes Remodelage Osseux et bioMatériaux – LHEA, IRIS-IBS Institut de Biologie en Santé, CHU d'Angers, 49933 Angers Cedex, France

ARTICLE INFO

Article history:
Received 4 September 2015
Accepted 25 April 2016
Available online 7 May 2016

Keywords:
BTX
Disuse osteoporosis
Epiphysis
Vector analysis
Porosity

ABSTRACT

Introduction: Botulinum toxin (BTX) injected in a muscle causes paralysis with a subsequent bone loss. It represents a model of disuse osteoporosis. Although bone loss has been regularly evaluated at the metaphysis of long bones, little is known concerning the bone changes occurring in the epiphysis.

Material and methods: Ten Copenhagen male rats received a single BTX injection in the *Mus quadriceps femoris* on the right side and unilateral paralysis developed in the following days. Animals were euthanized after 28 days; femur and tibia were harvested and analyzed by microCT. Vector analysis of porosity was applied to the 2D sections and produced a frontal image with mapping in pseudo-colors. This allows quantitative analysis at the epiphysis and metaphysis. ''Hot spot'' were evidenced and indicated bone loss. Quantitative analysis of these images was done by decomposition of the R, G and B planes and deriving the ratio of R + G pixels on the whole pixel number.

Results: At the metaphysis, this ratio was correlated with measurement of the bone volume obtained by microCT. At the epiphysis, which has a complex shape in 3D, the method easily identified the bone loss.

Discussion: Paralysis of a unilateral quadriceps induces bone loss at the metaphysis of the long bones. However, the epiphysis, having a reduced bone remodeling is also concerned by disuse. MicroCT analysis of this part of the bones is difficult due to its complex shape in 3D. Vector analysis is a new and robust method to quantify bone loss in such complex areas.

1. Introduction

Botulinum toxin (BTX) injections are now routinely used in clinical practice to temporarily paralyze muscle activity.[1] This leads to a transient muscle paralysis which is fully reversible in a few months.[2–4] BTX type A is produced by *Clostridium botulinum* that courses botulism, a food poisoning. BTX specifically inhibits the acetylcholine release at the neuromuscular synapse. BTX was initially proposed for its ability to reduce facial wrinkles.[5] BTX injections have also been proposed to treat muscle spasms in various locations.[6]

* Corresponding author at: GEROM – LHEA, IRIS-IBS Institut de Biologie en Santé, CHU d'Angers, University of Angers, 49933 Angers Cedex, France. Tel.: +33 244 68 83 49; fax: +33 244 68 83 51.
E-mail address: daniel.chappard@univ-angers.fr (D. Chappard).

http://dx.doi.org/10.1016/j.jasi.2016.04.002

We reported that a single BTX injection in the *mus quadriceps* can lead to a rapid bone loss due to the muscle paralysis.[7] The bone loss was evidenced at the upper tibia metaphysis and lower femoral metaphysis. These data were confirmed in other laboratory animals (mice, rabbits, cats, etc.) and by using various methods such as histomorphometry and microcomputed tomography (microCT).[8–11] In most of these papers, the metaphysis is analyzed because it contains a large amount of trabecular bone in the secondary spongiosa, immediately under the growth plate. However, bone loss also concerns cortical bone to a lesser extend.[12–15] It is now clear that muscle atrophy caused by the toxin leads to disuse with a secondary bone loss.[16] BTX is responsible for muscle paralysis in the injected muscle but also in the neighboring muscles.[11]

Bone loss induced by disuse is more intense in bones with a previous high remodeling. In the rat, bone loss was found more pronounced in the tibial metaphysis than at the femur's one.[7] However, bone remodeling of the epiphyseal bone has poorly been considered. Trabeculae of the epiphysis are thicker than in the metaphysis and the remodeling rate is lower.[17,18]

These characteristics have been attributed to the continuous loading of the epiphyses which preserves the thickness of their trabeculae throughout life.[17] However, the epiphyseal bone is difficult to analyze in rodents due to the reduced volume of this area. Histomorphometric analysis is not easy and microCT is difficult due to the complex shape of this bony subpart. Moreover, we developed of a new analysis technique applied to microCT sections of objects with a complex 3D shape (vector analysis of porosity).[19] In the present study, we conducted a vector analysis of porosity of the epiphyses and metaphyses of the femurs and tibae in a series of rats with BTX-induced paralysis of the *Mus quadriceps femoris*. The bones were analyzed by microCT and the sections were further treated by vector analysis.

2. Material and methods

2.1. Animals

Ten Copenhagen male rats weighing 485 ± 37 g were used in this study. Generation of the model has been described in detail elsewhere by our group.[7,20] Briefly, animals received a single injection of BTX (Botox® – Allergan France, 2 IU dissolved in 0.4 mL physiological saline) in the *Mus quadriceps femoris* of the right hindlimb (here after referred as the BTX-injected side). A 0.4 mL injection of saline was done in the left hindlimb (non-injected side). Paralysis of the right hindlimb was effective as early as 2 days post-injection and last up to 2 months followed by progressive recovery. Animals were sacrificed 28 days post-injection. This procedure was approved by the University of Angers ethical committee (Agreements 49028 and 01732.01) and performed in accordance with the European regulation for the use of animal in experimental procedures.

2.2. X-ray microcomputed tomography

MicroCT analysis was performed on tibias with a Skyscan 1172 microtomograph (Bruker-Skyscan, Kontich, Belgium) equipped with an X-ray tube working at 70 kV/100 μA. An isotropic voxel size was fixed at 13.4 μm, the rotation step at 0.25° and exposure was performed with a 0.5 mm aluminum filter. The CTAn Software (Skyscan, release 1.14.11) was used to measure the bone mass at the tibia upper metaphysis and the lower femur metaphysis after binarization with a global threshold. The first image selected for analysis was located just under the primary spongiosa (characterized by thin trabeculae) and then extended on 300 sections toward the bone shaft. The volume of interest (VOI) was designed by interactively drawing a polygon on each 2D section. Only a few

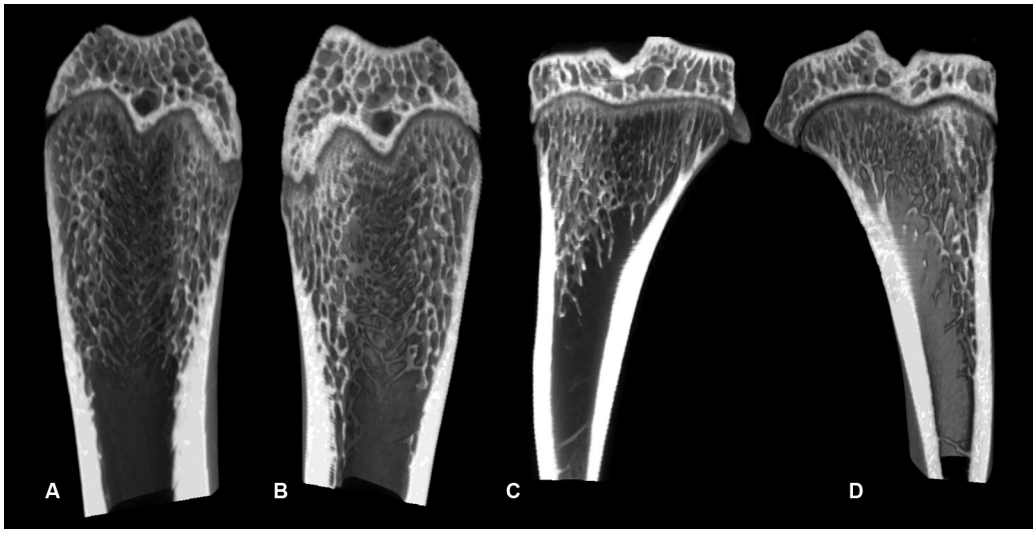

Fig. 1 – MicroCT image of bones of the same rat after BTX injection on the right side. (A) Right femur; (B) left femur; (C) right tibia; (D) left tibia. Note the reduced amount of the trabecular volume particularly in the right tibia metaphysis. Also note the larger trabeculae in the epiphyses than in the metaphysis.

Table 1 – Morphometric analysis of the tibiae and femurs by microCT and vector analysis.

	Femur		Tibia	
	BTX-injected	Non-injected	BTX-injected	Non-injected
BV/TV (%)	40.7 ± 0.5	48.7 ± 1.3[a]	41.1 ± 0.8	50.4 ± 0.5[a]
R metaphysis (%)	57.2 ± 1.9	47.3 ± 1.5[a]	60.6 ± 0.8	53.4 ± 1.3[a]
R epiphysis (%)	54.9 ± 1.9	35.9 ± 2.9[a]	49.0 ± 1.2	33.0 ± 1.4[a]

[a] Indicates a significant difference with the opposite side.

number of polygons need to be drawn (e.g. on the first section, several at the middle, and on the final section) since a routine facility calculated all the intermediary masks by interpolation. A first VOI containing only trabecular bone and marrow cavity was drawn and a global threshold was used to select the trabeculae.[21] The trabecular bone volume (BV/TV, in %) representing the percentage of the cancellous space occupied by trabecular bone was determined according to guidelines and nomenclature proposed by the American Society for Bone and Mineral Research.[22]

2.3. *Analysis of mandibular 3D porosity by a vector projection algorithm*

The stacks of binarized 2D sections were transferred to a lab-made software written in Matlab (Math Works, Natick, MA) release 7.10. The algorithm has been extensively described elsewhere.[19] Before analysis, the sesamoid bones were removed from the images because they produce artifactual results. On the binarized images, porosity was visible in white and bone in black. For each (*x*, *y*) binarized image of the stack, the pores (i.e. white pixels) which belong to the same image column *x* received the same pseudo-color according to a look up table (LUT). A LUT is a transfer function which determines what screen values correspond to image pixel intensity values at all *x*-*y* coordinates in the image. The representation of the LUT appears in Fig. 3. A 3D model was reconstructed from the subsequent colorized images the ImageJ 3D plugin (NIH, http://rsb.info.nih.gov/ij/index.html). A frontal image was saved in the tif format with the colorized LUT and analyzed by ImageJ. With this method, the large porous areas (indicating the disappearance of trabeculae) are in "hot colors" (i.e. red, orange and yellow) and areas rich in trabeculae or cortical bone appear in blue ("cold colors"). The method to analyze quantitatively RGB images was proposed by several authors and is based on the 3 histograms of the image.[23,24] In the additive RGB color model (Red-Green-Blue), each image can be decomposed in 3 planes (red, green and blue). The histogram of each bit plane was obtained with ImageJ and transferred to an Excel spreadsheet (Microsoft Co). Then, only values comprised between 20 and 255 gray level were selected to discard irrelevant data. They were converted in percent of the whole number of pixels and the ratio *R* of the (red + green) pixels to the whole number of pixels was derived. This method allows determination of the fraction of the image containing "hot colors" because yellow is obtained by adding red and green pixels values in the RGB mode. *R* was measured separately in the metaphysis (an area corresponding to the BV/TV measurements done in 3D) and the epiphysis of each bone.

2.4. *Statistical analysis*

Statistical analysis was performed using the Systat statistical software release 13.0 (Systat Software Inc., San Jose, CA). All

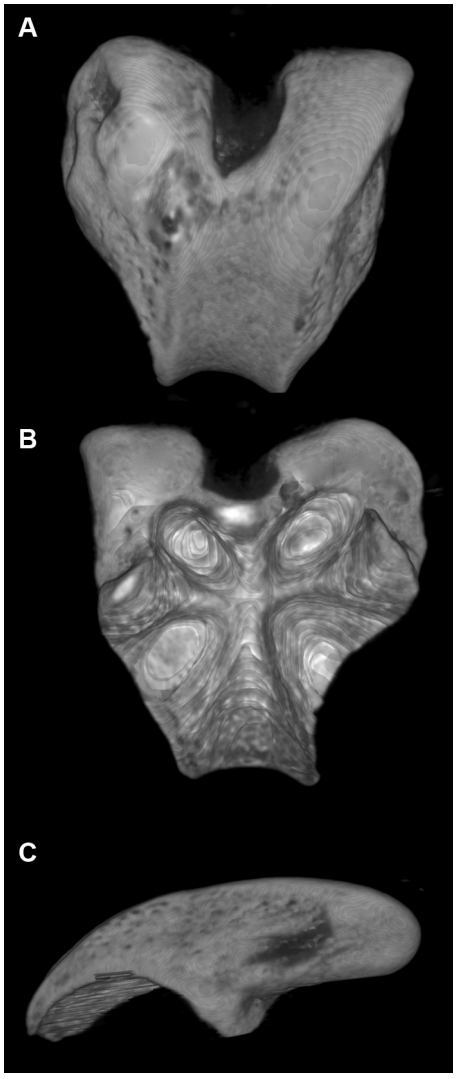

Fig. 2 – MicroCT images of a femoral rat epiphysis. The image was obtained by removal image by image the primary and secondary spongiosa on the whole stack of images using Photoshop CS5 (Adobe). (A) Upper view showing the two condyles and the intercondylar notch. (B) Lower view showing the four expansions of the primary spongiosa and their impingement deep inside the epiphysis. (C) Lateral view with the presence of horns in various directions.

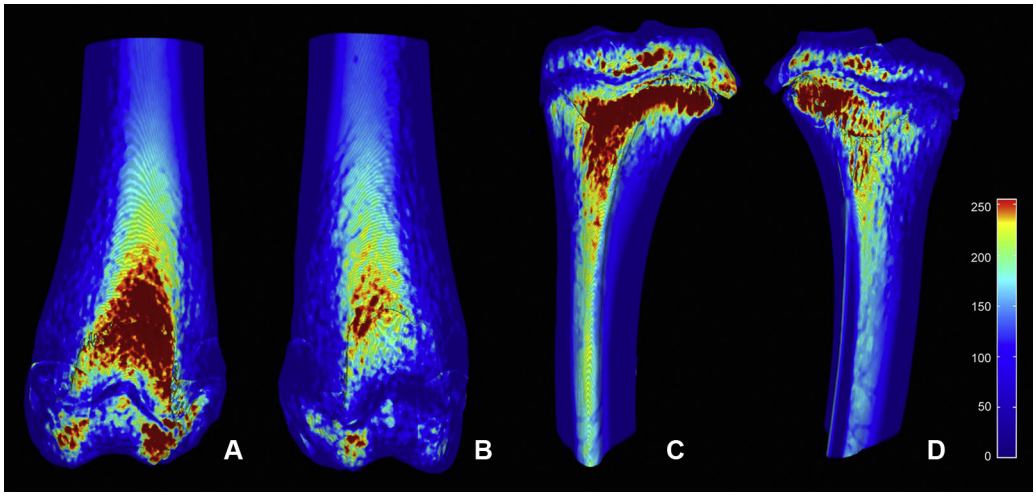

Fig. 3 – Analysis of the same bones than in Fig. 1, by vector analysis. The presence of "red spots" indicates areas where porosity is increased (A) right femur; (B) left femur; (C) right tibia; (D) left tibia. The LUT appears on the right side of the figure.

data were expressed as mean ± standard error of the mean (SEM). Differences between the right and left bones were compared using the Mann and Whitney's *U* test. Differences were considered significant when $p < 0.05$.

3. Results

3.1. *Assessment of bone mass on microCT images of the metaphysis*

Fig. 1 illustrates the bone loss in these two bones from the same animal. The trabecular bone volume was markedly decreased at the metaphysis of the two bones on the BTX injected side. A −16.4% decrease was observed at the femur and a −18.4% at the tibia (Table 1). Fig. 2 illustrates the complex shape of a femoral epiphysis in 3D after interactive elimination of the primary and the secondary spongiosa from the stack of 2D images containing. Each image was processed separately. It is likely that it is impossible to select the trabecular bone in this area because softwares cannot adapt to such complicated boundaries.

3.2. *Assessment of bone porosity on images with vector analysis*

Fig. 3 illustrates the aspect of the femurs and tibia of the same rat imaged after vector analysis of porosity. The highest porous zones (corresponding to areas with an increased trabecular resorption) appear in "hot colors" i.e. red to yellow. The bone loss is easily demonstrated in the metaphyses of both bones. In the epiphyses, the presence of "hot spots" is also clearly evidenced and corresponds to a bone loss. In all the rats of the series, the maximum areas with increased porosity were observed at the inner femoral condyle. In the tibia, the "hottest areas" were also observed at the inner plateau.

The difference in *R* reached 20.9% at the femoral metaphysis and 13.5% at the tibial metaphysis. In the epiphyses, the difference was 52.9% at the femur and 48.4% at the tibia.

The histograms of the Red, Green and Blue planes of metaphyseal ROIs in the injected and non-injected side of a femur appear in Fig. 4. On the non-injected side, the histogram frequency exhibits a large peak for the blue component while

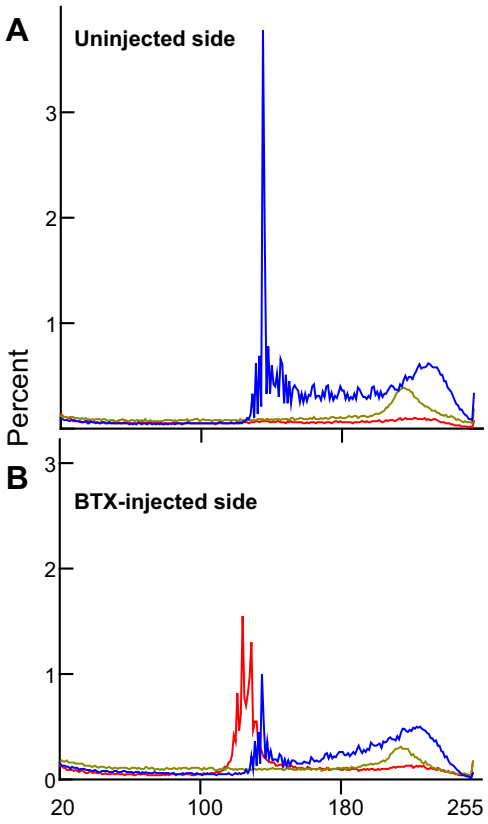

Fig. 4 – The Red, Green and Blue histograms of the metaphysis of the femur in (A) the un-injected side (left limb) and (B) the injected side (right limb). Note the increase number of red pixels in the histogram and the reduction in the percent of blue pixels after BTX injection. Each histogram is figured with its representative color.

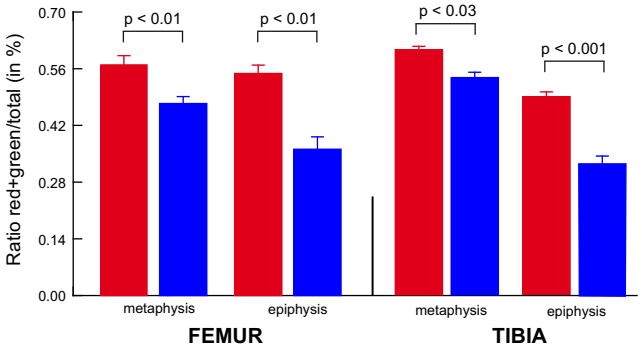

Fig. 5 – Quantitative analysis of the ratio (red + green) pixels on the total number of pixels in the metaphysis and epiphysis of the femur and tibia of rats having received a BTX injection in the *Mus quadriceps femoris*. BTX-injected side in red (right); non-injected side in blue (left).

the green and red histograms are more flattened. On the BTX-injected side (Fig. 4B), the peak of the blue histogram is markedly reduced and the red histogram exhibits a large peak. The *R* ratio is illustrated in Fig. 5 and Table 1 in the different bones and their metaphyseal and epiphyseal subparts. Noteworthy, BV/TV measured by microCT and *R*, estimated at the metaphysis were well linearly correlated ($r = -0.65$; $p = 0.001$).

4. Discussion

Striated muscles are under the control of the voluntary nervous system which controls body movements. The motoneurons of the spinal cord transmit information to the muscles via their axon which ends at the neuromuscular synapse. Acetylcholine is the neurotransmitter released by the axon and BTX blocks its release by destroying the intracellular SNARE system involved in the fusion of the synaptic vesicles with the cell membrane.[2–4] The paralysis occurs within 2 days after injection of the toxin and the muscle function recovery is observed within two months. Paralysis causes disuse of the injected limb leading to a rapid bone loss.[7] The effect of BTX on bone loss is cumulative with other factors known to reduce bone mass such as castration.[25,26] or hind limb unloading.[27] At the bone cell level, bone loss is due to a sudden increase in osteoclast number associated with a progressive decline of the osteoblastic formation of new bone.[28] Since the original description of the model, at least 40 publications have been presented and pharmacological or physical counter measures have been evaluated.[29] However, up to now, little consideration has been paid to the epiphyses because this bone subpart is difficult to analyze. Because of the heterogeneity in trabecular repartition and the very complex shape of this bone (see Fig. 2), a very limited number of studies have been done on bone loss in this area in animal models of osteoporosis. In the present study, we performed a "virtual dissection" of a femoral epiphysis to show the 3D complexity of a femoral epiphysis and to explain why it is impossible to select the whole trabecular bone inside the cortical shell of the epiphysis. Although some studies have presented data on bone remodeling at the epiphysis in laboratory animals, they are most often concerned with 2D microCT images,[30] histological sections,[31,32] or scanning electron microscopic images.[31] To our knowledge, only two papers have presented a quantitative analysis of trabecular bone by microCT at the epiphysis but determination of the VOI was poorly described and no 3D model was presented.[33,34] Here, the bone loss induced by the BTX-related disuse was confirmed at the metaphysis of mature rat bones by a quantitative analysis using the dedicated software available for microCT. Vector analysis of porosity was initially developed by our group to analyze the complexity of the pores in various biomaterials presenting a complex shape.[19] The method was also successfully used to characterize the alveolar bone loss at the mandible in rats with paralysis of masticatory muscles.[35] A very similar approach was presented previously to appreciate the thinning of cortical bone at the hip on human CT scans with mapping pseudo-colors at the surface of the 3D model.[36,37] Here, we found that vector analysis could be applied to evaluate the bone loss in the metaphysis and epiphysis of rats in the BTX model. MicroCT values and *R* were well correlated in the metaphysis, making the method valid to extrapolate the results to the epiphysis. However, the variations in *R* are not comparable between different types of bones because the bone width influences the parameter. So, *R* can only be used to compare changes occurring in the same bone. In addition, the method allows an immediate visual perception of the bone loss in these two skeletal pieces.

5. Conclusion

BTX induces bone loss after paralysis of a single muscle. It occurs both at the femur and tibia on which the different heads of the muscle are inserted. Disuse causes bone loss at the trabecular envelope of the metaphysis and epiphysis. Vector analysis of porosity can be quantified by analysis of the RGB histograms of the images.

Conflicts of interest

The authors have none to declare.

Acknowledgments

This work was made possible by grants from National ministry of Research. Many thanks to Mrs. Lechat for secretarial assistance.

Appendix A. Supplementary data

Supplementary data associated with this article can be found, in the online version, at doi:10.1016/j.jasi.2016.04.002.

REFERENCES

1. Brin MF, Fahn S, Moskowitz C, et al. Localized injections of botulinum toxin for the treatment of focal dystonia and hemifacial spasm. *Mov Disord*. 1987;2:237–254.
2. Poulain B. Molecular mechanism of action of tetanus toxin and botulinum neurotoxins. *Pathol Biol*. 1994;42:173–182.
3. Rossetto O, Pirazzini M, Bolognese P, Rigoni M, Montecucco C. An update on the mechanism of action of tetanus and botulinum neurotoxins. *Acta Chem Slov*. 2011;58:702–707.
4. Tighe AP, Schiavo G. Botulinum neurotoxins: mechanism of action. *Toxicon*. 2013;67:87–93.
5. Fagien S. Botox for the treatment of dynamic and hyperkinetic facial lines and furrows: adjunctive use in facial aesthetic surgery. *Plast Reconstr Surg*. 1999;103:701–713.
6. Ihde SKA, Konstantinovic VS. The therapeutic use of botulinum toxin in cervical and maxillofacial conditions: an evidence-based review. *Oral Surg Oral Med Oral Pathol Oral Radiol Endod*. 2007;104:e1–e11.
7. Chappard D, Chennebault A, Moreau M, Legrand E, Audran M, Basle MF. Texture analysis of X-ray radiographs is a more reliable descriptor of bone loss than mineral content in a rat model of localized disuse induced by the *Clostridium botulinum* toxin. *Bone*. 2001;28:72–79.
8. Olabisi R, Best TM, Vanderby Jr R, Petr S, Noonan KJ. Effects of botulinum toxin A on functional outcome during distraction osteogenesis. *J Orthop Res*. 2007;25:656–664.
9. Rafferty KL, Liu ZJ, Ye W, et al. Botulinum toxin in masticatory muscles: short-and long-term effects on muscle, bone, and craniofacial function in adult rabbits. *Bone*. 2012;50:651–662.
10. Warner SE, Sanford DA, Becker BA, Bain SD, Srinivasan S, Gross TS. Botox induced muscle paralysis rapidly degrades bone. *Bone*. 2006;38:257–264.
11. Yaraskavitch M, Leonard T, Herzog W. Botox produces functional weakness in non-injected muscles adjacent to the target muscle. *J Biomech*. 2008;41:897–902.
12. Ausk BJ, Huber P, Srinivasan S, et al. Metaphyseal and diaphyseal bone loss in the tibia following transient muscle paralysis are spatiotemporally distinct resorption events. *Bone*. 2013;57:413–422.
13. Bouvard B, Mabilleau G, Legrand E, Audran M, Chappard D. Micro and macroarchitectural changes at the tibia after botulinum toxin injection in the growing rat. *Bone*. 2012;50:858–864.
14. Grimston SK, Goldberg DB, Watkins M, Brodt MD, Silva MJ, Civitellit R. Connexin43 deficiency reduces the sensitivity of cortical bone to the effects of muscle paralysis. *J Bone Miner Res*. 2011;26:2151–2160.
15. Libouban H, Blouin S, Moreau MF, Baslé MF, Audran M, Chappard D. Effects of risedronate in a rat model of osteopenia due to orchidectomy and disuse: densitometric, histomorphometric and microtomographic studies. *Micron*. 2008;39:998–1007.
16. Manske SL, Boyd SK, Zernicke RF. Muscle changes can account for bone loss after botulinum toxin injection. *Calcif Tissue Int*. 2010;87:541–549.
17. Frost HM, Jee WS. Perspectives: a vital biomechanical model of the endochondral ossification mechanism. *Anat Rec*. 1994;240:435–446.
18. Silvestrini G, Ballanti P, Leopizzi M, et al. Effects of intermittent parathyroid hormone (PTH) administration on SOST mRNA and protein in rat bone. *J Mol Histol*. 2007;38:261–269.
19. Chappard D, Stancu IC. Porosity imaged by a vector projection algorithm correlates with fractal dimension measured on 3D models obtained by microCT. *J Microsc*. 2014. http://dx.doi.org/10.1111/jmi.12212.
20. Blouin S, Gallois Y, Moreau MF, Basle MF, Chappard D. Disuse and orchidectomy have additional effects on bone loss in the aged male rat. *Osteoporos Int*. 2007;18:85–92.
21. Tassani S, Korfiatis V, Matsopoulos G. Influence of segmentation on micro-CT images of trabecular bone. *J Microsc*. 2014;256:75–81.
22. Dempster DW, Compston JE, Drezner MK, et al. Standardized nomenclature, symbols, and units for bone histomorphometry: a 2012 update of the report of the ASBMR Histomorphometry Nomenclature Committee. *J Bone Miner Res*. 2013;28:2–17.
23. Gerin C, Pallud J, Deroulers C, et al. Quantitative characterization of the imaging limits of diffuse low-grade oligodendrogliomas. *Neuro Oncol*. 2013;15:1379–1388.
24. Seo Y, Choi S, Kim H, Hong K-S. Where are the ball and players? Soccer game analysis with color-based tracking and image mosaick. *Image Anal Process*. 1997;196–203. Springer.
25. Blouin S, Gallois Y, Moreau MF, Baslé MF, Chappard D. Disuse and orchidectomy have additional effects on bone loss in the aged male rat. *Osteoporos Int*. 2007;18:85–92.
26. Libouban H, Blouin S, Moreau M-F, Baslé MF, Audran M, Chappard D. Effects of risedronate in a rat model of osteopenia due to orchidectomy and disuse: densitometric, histomorphometric and microtomographic studies. *Micron*. 2008;39:998–1007.
27. Ellman R, Grasso DJ, van Vliet M, et al. Combined effects of botulinum toxin injection and hind limb unloading on bone and muscle. *Calcif Tissue Int*. 2014;94:327–337.
28. Marchand-Libouban H, Le Drevo MA, Chappard D. Disuse induced by botulinum toxin affects the bone marrow expression profile of bone genes leading to a rapid bone loss. *J Musculoskelet Neuronal Interact*. 2013;13:27–36.
29. Grubbe M, Thomsen J, Nyengaard J, Duruox M, Brüel A. Growth hormone mitigates loss of periosteal bone formation and muscle mass in disuse osteopenic rats. *J Musculoskelet Neuronal Interact*. 2014;14:473–483.
30. Borrelli Jr J, Zaegel MA, Martinez MD, Silva MJ. Diminished cartilage creep properties and increased trabecular bone density following a single, sub-fracture impact of the rabbit femoral condyle. *J Orthop Res*. 2010;28:1307–1314.
31. Baldock PAJ, Morris HA, Moore RJ, Need AG, Durbridge TC. Prepubertal oophorectomy limits the accumulation of cancellous bone in the femur of growing rats with long-term effects on metaphyseal bone architecture. *Calcif Tissue Int*. 1998;62:244–249.
32. Tomaszewska E, Dobrowolski P, Puzio I. Morphological changes of the cartilage and bone in newborn piglets evoked by experimentally induced glucocorticoid excess during pregnancy. *J Anim Physiol Anim Nutr*. 2013;97:785–796.
33. Garman R, Gaudette G, Donahue LR, Rubin C, Judex S. Low-level accelerations applied in the absence of weight bearing can enhance trabecular bone formation. *J Orthop Res*. 2007;25:732–740.
34. Squire M, Brazin A, Keng Y, Judex S. Baseline bone morphometry and cellular activity modulate the degree of bone loss in the appendicular skeleton during disuse. *Bone*. 2008;42:341–349.
35. Kün-Darbois JD, Libouban H, Chappard D. Botulinum toxin in masticatory muscles of the adult rat induces bone loss at the condyle and alveolar regions of the mandible associated with a bone proliferation at a muscle enthesis. *Bone*. 2015;77:75–82.
36. Poole KE, Treece GM, Mayhew PM, et al. Cortical thickness mapping to identify focal osteoporosis in patients with hip fracture. *PLoS ONE*. 2012;7:e38466.
37. Treece GM, Gee AH, Mayhew P, Poole K. High resolution cortical bone thickness measurement from clinical CT data. *Med Image Anal*. 2010;14:276–290.